Pressure-driven phase transition from antiferromagnetic semiconductor to nonmagnetic metal in the two-leg ladders AFe_2X_3 (A = Ba, K; X = S, Se)

Yang Zhang,[1] Lingfang Lin,[1] Jun-Jie Zhang,[1] Elbio Dagotto,[2,3] and Shuai Dong[1,*]
[1]*School of Physics, Southeast University, Nanjing 211189, China*
[2]*Department of Physics and Astronomy, University of Tennessee, Knoxville, Tennessee 37996, USA*
[3]*Materials Science and Technology Division, Oak Ridge National Laboratory, Oak Ridge, Tennessee 37831, USA*
(Received 15 November 2016; revised manuscript received 24 January 2017; published 31 March 2017)

The recent discovery of superconductivity in $BaFe_2S_3$ [H. Takahashi *et al.*, Nat. Mater. **14**, 1008 (2015)] has stimulated considerable interest in 123-type iron chalcogenides. This material is the first reported iron-based two-leg ladder superconductor, as opposed to the prevailing two-dimensional layered structures of the iron superconductor family. Once the hydrostatic pressure exceeds 11 GPa, $BaFe_2S_3$ changes from a semiconductor to a superconductor below 24 K. Although previous calculations correctly explained its ground-state magnetic state and electronic structure, the pressure-induced phase transition was not successfully reproduced. In this work, our first-principles calculations show that with increasing pressure the lattice constants as well as local magnetic moments are gradually suppressed, followed by a first-order magnetic transition at a critical pressure, with local magnetic moments dropping to zero suddenly. Our calculations suggest that the self-doping caused by electrons transferred from S to Fe may play a key role in this transition. The development of a nonmagnetic metallic phase at high pressure may pave the way to superconductivity. As extensions of this effort, two other 123-type iron chalcogenides, KFe_2S_3 and KFe_2Se_3, have also been investigated. KFe_2S_3 also displays a first-order transition with increasing pressure, but KFe_2Se_3 shows instead a second-order or weakly first-order transition. The required pressures for KFe_2S_3 and KFe_2Se_3 to quench the magnetism are higher than for $BaFe_2S_3$. Further experiments could confirm the predicted first-order nature of the transition in $BaFe_2S_3$ and KFe_2S_3, as well as the possible metallic/superconductivity state in other 123-type iron chalcogenides under high pressure.

DOI: 10.1103/PhysRevB.95.115154

I. INTRODUCTION

Since the discovery of superconductivity in fluorine-doped LaFeAsO [1], iron pnictides and chalcogenides have rapidly developed into one of the main branches of research in the field of unconventional superconductors [2–4]. Almost all previously reported iron-based superconductors have similar crystal structures, involving a slightly distorted two-dimensional Fe square lattice [5–8], where each Fe atom is caged in a tetrahedral structure. The magnetism of the nonsuperconducting parent state is primarily given by the collinear stripelike order, namely, the C-type antiferromagnetic (C-AFM) order, although some exceptions exist such as in FeTe, FeSe, KFe_2Se_2, and $K_2Fe_4Se_5$ [9–19]. The structural and magnetic similarities of all these iron-based superconductors suggest common physical mechanisms leading to their magnetic and superconducting properties, despite the different ratios of the atomic elements involved.

However, recently, iron chalcogenides with a different structure, the so-called 123-type AFe_2X_3 (A=K, Cs, Rb, Ba; X=S, Se, Te), have drawn considerable attention [20–27]. These materials display unique quasi-one-dimensional two-leg ladder iron structures [see Fig. 1(a)] that are clearly qualitatively distinct from the other extensively studied iron pnictides/chalcogenides with iron layers. At least from the perspective of the electronic structure, the frequently mentioned Fermi surface nesting effect involving two pocket cylindrical Fermi surfaces (corresponding to the quasi-two-dimensional structure) in several iron pnictides/chalcogenides cannot be relevant in these ladder systems [2,4–7]. Thus, the reduced dimensionality of the iron network makes AFe_2X_3 a physically fascinating material that deserves further experimental and theoretical scrutiny. In fact, the two-leg ladders made of Fe atoms remind us of the previously studied two-leg ladders superconducting cuprates [28,29]. In the past, the study of cuprate ladders greatly illuminated the physics of Cu oxides, primarily because theoretical calculations involving the model Hamiltonian can be carried out with good accuracy in chains and ladders, and thus, accurate theory-experiment comparisons can be done. A similar important impact of iron ladders on the field of iron superconductors is now to be expected.

In this family of ladder materials, $BaFe_2Se_3$ was the first compound reported to be superconducting at approximately 11 K [20]. However, others experiments claimed the material was a semiconductor with the observed superconductivity probably induced by impurities [22]. Even under these circumstances, one of our previous studies predicted an interesting property, namely, that its block-type antiferromagnetic state is multiferroic due to magnetostriction effects [30,31]. The theoretically predicted polar structure has indeed been verified by a subsequent neutron study [32]. In addition, doping of K in the Ba site changes the ground state to the so-called CX-type antiferromagnetism [CX-AFM; see Fig. 1(b)] [23]. Such CX-AFM order was also predicted to be the ground state of $BaFe_2S_3$, which was later also confirmed using neutron techniques [33]. Under ambient conditions, $BaFe_2S_3$ has a semiconducting ground state with a very small gap of about 0.06–0.07 eV [34,35]. The most striking recent experimental discovery is that high pressure can drive $BaFe_2S_3$ to become superconducting when the hydrostatic pressure exceeds about

*Corresponding author: sdong@seu.edu.cn

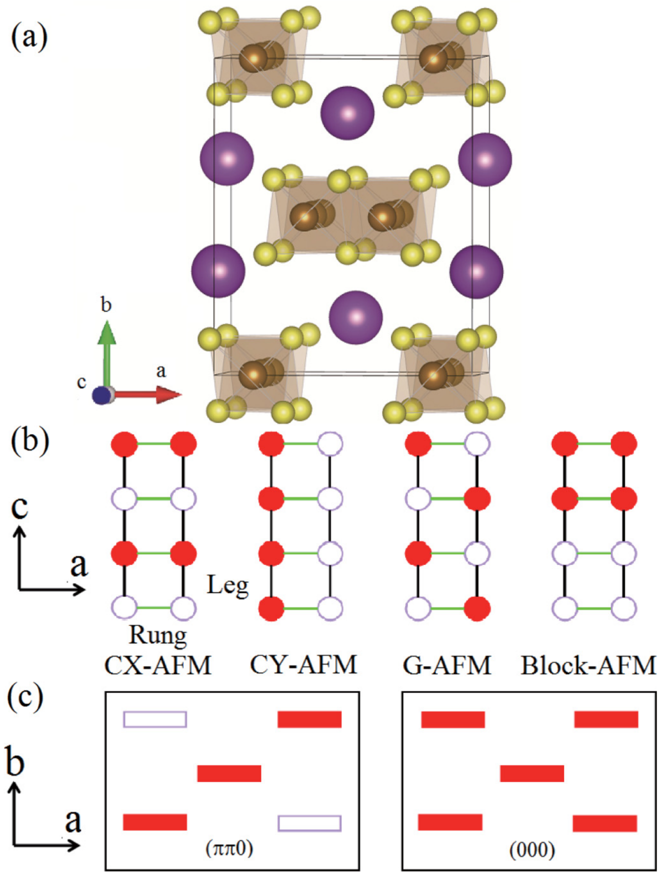

FIG. 1. (a) Schematic crystal structure of AFe_2X_3. Purple: A, e.g., Ba or K; yellow: X, e.g., S or Se; brown: Fe. (b) Sketch of the possible spin configurations that could be stabilized in two-leg iron ladders. Spin up and spin down are distinguished by different colors. (c) Schematic of the three-dimensional magnetic $(\pi,\pi,0)$ and $(0,0,0)$ configurations between ladders.

11 GPa [33] and its highest T_c can reach 24 K at 13.5 GPa [36].

A subsequent density functional theory (DFT) study by Suzuki *et al.* on $BaFe_2S_3$ confirmed the CX-AFM nature of the magnetic state (see also our earlier work [30]) as well as its semiconducting behavior under ambient conditions [37]. However, the pressure-induced magnetic to nonmagnetic transition (as phenomenologically required by superconductivity) was not obvious from that DFT study, although the calculation indeed showed a semiconductor-metal transition at about 5 GPa. In those previous DFT calculations, the magnetism persisted with only a small suppression upon increasing pressure. This problem might be due to the process followed to allow the relaxation of the crystal structure under pressure since for simplicity only the positions of sulfur atoms were optimized in the x-y plane in that previous study, which is sufficient for a qualitative analysis. However, in our study presented below all atomic positions were simultaneously relaxed, allowing us to be not only qualitative but also quantitative in our analysis.

In the present publication, the magnetic properties, electronic structure, and pressure effects corresponding to $BaFe_2S_3$ are revisited using first-principles DFT calculations. Our results can be divided in two classes. First, results similar to those from previous DFT efforts and experiments for the ambient conditions have been obtained and confirmed. Second, a semiconductor-metal transition accompanying the quenching of magnetism has been observed, in good agreement with experimental observations. This phase transition is probably of first order because we observe a sudden drop in the iron's magnetic moment and also anomalies in the crystal structure. More specifically, one of our most important results is that the underlying physics of this transition lies in the modifications by pressure of the effective electronic density of the iron network of relevance. Thus, the net effect of increasing pressure is equivalent to doping charge into the iron atoms, a nontrivial effect difficult to deduce from the existing experimental information. Following these arguments, two additional AFe_2X_3 materials (KFe_2S_3 and KFe_2Se_3) have also been studied theoretically using a similar procedure. The quenching of magnetic moments and metallic phases have also been obtained for the cases of both KFe_2S_3 and KFe_2Se_3, although at higher pressures. The theoretical observation of these pressure-induced transitions suggests possible pressure-induced superconducting states also in KFe_2S_3 and KFe_2Se_3 in analogy with what occurs in $BaFe_2S_3$, although we cannot explicitly prove these predictions due to the limitations of DFT techniques in addressing superconductivity. We expect our results to motivate experimental efforts for their confirmation.

II. METHODS

The DFT calculations are performed based on the generalized gradient approximation (GGA) with the projector augmented-wave (PAW) potentials, as implemented in the Vienna Ab initio Simulation Package (VASP) [38–41]. The Perdew-Burke-Ernzerhof (PBE) exchange function has been adopted. The plane-wave cutoff is 500 eV. The k-point mesh is $4\times3\times6$ for the minimum crystalline unit cell, which is accordingly adapted for the various magnetic cells studied [e.g., $2\times6\times2$ for CX-AFM $(\pi,\ \pi,\ 0)$]. Starting from experimental values, both the lattice constants and atomic positions are fully relaxed until the force on each atom is below 0.01 eV/Å.

To study the magnetic properties, various possible (in-ladder) magnetic structures are imposed on the Fe ladders, as shown in Fig. 1(b). Despite the in-ladder correlation, the magnetic correlation between ladders can also slightly affect the physical properties. Therefore, besides the simplest $(0,0,0)$ order, the $(\pi,\ \pi,\ 0)$ order is also studied, as indicated in Fig. 1(c).

In addition to the standard DFT calculation, the maximally localized Wannier functions (MLWFs) have also been employed to fit five Fe $3d$ bands and the Fermi surface, using the WANNIER90 packages [42].

Several previous DFT studies found that even the pure GGA (or local spin-density approximation) procedure overestimates the local magnetic moments in iron pnictides and chalcogenides [16,43–46]. Thus, using GGA+U with a positive U will render this inconsistency even more serious. Thus, in some studies, a negative U correction was adopted to better describe the 122-type Fe-based materials [47,48]. Alternatively, the exchange and correlation kernels were rescaled by an appropriate factor [49]. In the present study, both GGA+U and pure GGA have been tested, and we found that the latter provides a better description of $A\mathrm{Fe_2X_3}$ (regarding its crystalline constants, magnetic moments, and band gaps). For this reason, only the pure GGA results will be presented in the rest of this paper.

III. RESULTS AND DISCUSSION

A. Magnetism and electronic structure of $\mathrm{BaFe_2S_3}$

Our main DFT results with regards to the magnetic and electronic properties of the $\mathrm{BaFe_2S_3}$ ladder can be summarized by four statements:

(1) Without the external pressure, both the lattice constants and atomic positions were fully optimized in the presence of magnetism. In the pure GGA calculation, the CX-AFM (π, π, 0) state has the lowest energy among all candidate configurations investigated, in agreement with experiments. The CX-AFM (0, 0, 0) is only slightly higher in energy by 6.3 meV/Fe, which is reasonable considering the similarity between these two CX-AFM configurations.

(2) Even the pure GGA result gives a magnetic moment ($2.08\mu_\mathrm{B}$/Fe) that is slightly higher than the experimental one ($\sim 1.2\mu_\mathrm{B}$/Fe at low temperature, as measured by neutron scattering [33]). This overestimated local moment is quite common in DFT calculations of iron-based superconductors [43–45], which may be due to the coexistence of localized Fe spins and itinerant electrons [50]. Note that this calculated value also depends on how large the Wigner-Seitz radius of the iron atom is set to be. Thus, the inconsistency described above may partially originate from the methodological difference between the VASP procedure and neutron experiments.

(3) For the experimentally relevant CX-AFM (π, π, 0) state, the pure GGA calculation gives a small gap of 0.088 eV, which agrees with the experimental value (0.06–0.07 meV) [34,35] and previous DFT results [37].

(4) According to the calculated density of states (DOS; not shown), the bands near the Fermi levels are highly hybridized between Fe 3d orbitals and S 3p orbitals. Such hybridization is quite common in iron pnictides and chalcogenides.

B. Pressure-induced transition in $\mathrm{BaFe_2S_3}$

Although previous DFT calculations correctly reproduced the magnetic ground state and electronic structure of $\mathrm{BaFe_2S_3}$, the pressure-induced magnetic-nonmagnetic transition (presumably also associated with superconductivity, although beyond the DFT scope) was not reproduced [37], as explained above. Below, these pressure effects will be revisited using DFT.

By increasing the hydrostatic pressure in the calculation, our energies and Fe magnetic moments are summarized in Figs. 2(a) and 2(b). For all magnetic orders, the local moments decrease with pressure, but the CX-AFM (π, π, 0) state always has the lowest energy. When the pressure reaches 10.8 GPa (very close to the experimental critical pressure [33,36]), the *static values* of the local moments drop to zero. Meanwhile, the system becomes metallic. Such a nonmagnetic metallic phase provides the conditions for superconductivity if there are still antiferromagnetic

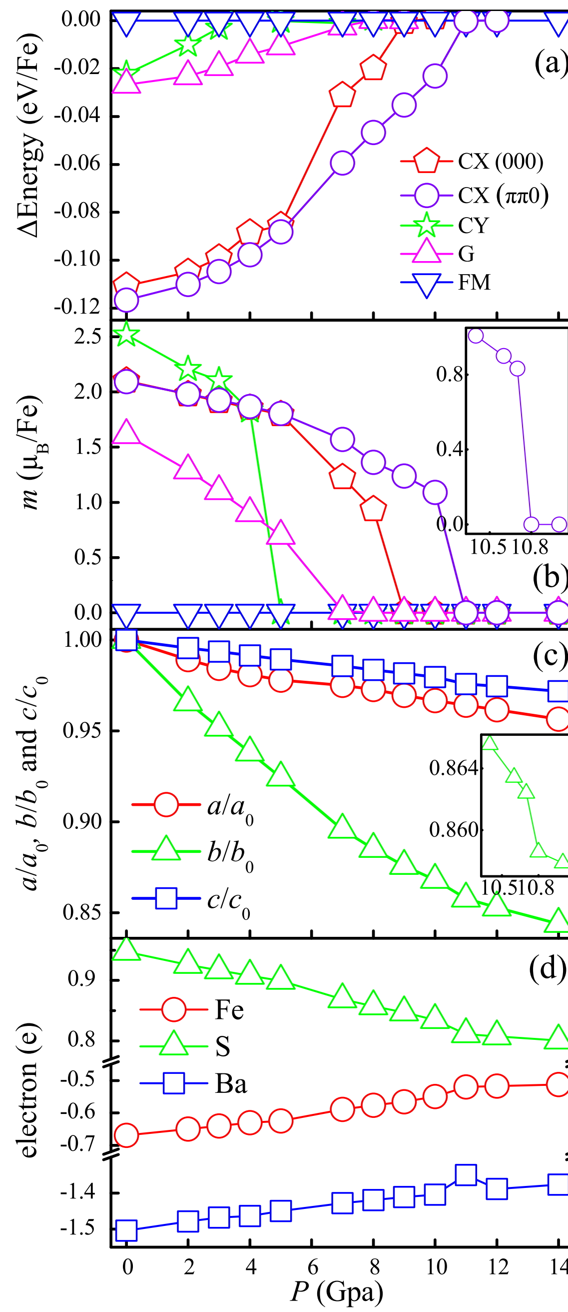

FIG. 2. DFT results corresponding to $\mathrm{BaFe_2S_3}$ as a function of pressure. (a) Energy difference (per Fe) of various magnetic orders with respect to the ferromagnetic (FM) state. (b) Local magnetic moments of Fe. Inset: a magnified view near the transition. (c) Lattice constants normalized to the original ones for the CX-AFM (π, π, 0) state. Inset: a magnified view near the transition. (d) Bader charge analysis.

fluctuations present (although short-range magnetic quantum fluctuations also cannot be captured in the DFT calculation). In this sense, without fine-tuning parameters, our calculation correctly reproduces the antiferromagnetic-to-nonmagnetic transition. Furthermore, we found that the quenching of magnetic moments occurs as in a first-order transition, with a sudden drop from $0.83\mu_\mathrm{B}$/Fe to zero at 10.8 GPa [inset of Fig. 2(b)].

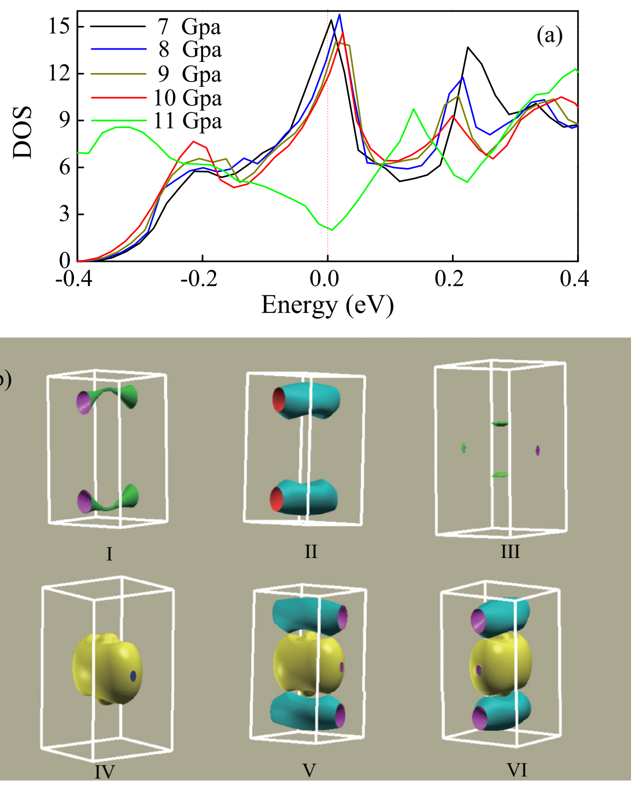

FIG. 3. (a) Evolution of the DOS near the Fermi level with increasing pressure. Below the critical pressure, a Van Hove singularity appears at the Fermi level, but it suddenly disappears at the critical pressure. Only the spin-up channel is shown because the spin-down channel is exactly identical since the system is either antiferromagnetic or nonmagnetic. (b) Fermi surfaces at 11 GPa. Panels I–IV are individual Fermi surfaces. Panels V and VI are the total Fermi surfaces viewed from different orientations.

Figure 2(c) shows the compressibility, i.e., the lattice constants normalized to the ambient ones. The *b*-axis lattice is the softest, while the *c*-axis lattice is the hardest, as in experiments [33]. Such anisotropic compressibility can be intuitively understood considering the loose space between ladders and the compact bonds along ladders. The first-order character of the transition at 10.8 GPa can also be observed in the lattice structure (especially for the lattice constant along the *b* axis), as emphasized in the inset of Fig. 2(c). This first-order characteristic was not reported previously and could be verified in future experiments.

According to the Bader charge analysis [Fig. 3(d)] [51–53], there is a significant charge transfer (~ 0.15 electron) from S to Fe when increasing pressure from 0 to 12 GPa. This tendency is equivalent to the effects of electron doping by, for example, chemical substitution, which is the standard procedure to generate superconductivity from a magnetic parent compound. In this sense, it is reasonable to suspect that the superconductivity observed in $BaFe_2S_3$ is probably induced by electron doping, in analogy with the superconductivity triggered by F doping in LaFeAsO. This is also quite similar to what happened in previous investigations of the Cu ladders, where a transfer of charge from chains to ladders triggers superconductivity [54]. In summary, our calculations suggest that the superconductivity of $BaFe_2S_3$ is probably caused by self-doping of electrons into the iron network. This effect can occur in addition to the previously proposed scenario based on the broadening of the electronic bandwidth by pressure [33]. Only further experimental work can clarify which of the two tendencies is more dominant to generate superconductivity.

A careful analysis of the DOS at the Fermi level just before the critical pressure finds a sharp peak, i.e., a Van Hove singularity, which suddenly drops to become a valley around 11 GPa, as shown in Fig. 2(a). The first-order magnetic-nonmagnetic transition leads to the sudden disappearance of this Van Hove singularity since electronic bands are seriously reconstructed at the critical pressure. The Fermi surface at 11 GPa is shown in Fig. 2(b), with four bands crossing the Fermi level. Two of them nest around the Γ point, while the other two are isolated.

C. Pressure-induced transition in KFe_2S_3

Until now, $BaFe_2S_3$ was the only experimentally confirmed superconductor in the 123-type series of iron ladders. As a consequence, it is interesting to investigate whether there are other 123-type iron ladders that can also potentially become superconductors. KFe_2S_3 is a sister member of $BaFe_2S_3$, where the nominal valence of Fe is higher by $+0.5$. Experimentally, KFe_2S_3 has been synthesized [55] but its detailed physical properties have not been reported, particularly under high pressure. Structurally, this K-based 123 ladder is similar to $BaFe_2S_3$, with the same *Cmcm* group.

Here, DFT calculations have been performed also on KFe_2S_3. In this study we have found that the magnetic ground state is also of the CX-AFM type. Moreover, the local magnetic moment is about $2.3\mu_B$/Fe in the pure GGA calculations. Compared to that of $BaFe_2S_3$, the band gap of KFe_2S_3 (~ 0.51 eV in pure GGA calculations) is slightly larger. According to the atomically resolved DOS (not shown), the states near the Fermi level are also primarily contributed by the Fe $3d$ orbitals, which are also highly hybridized with the S $3p$ orbitals.

According to the Bader charge analysis, the electronic densities at the Fe and S sites in KFe_2S_3 are lower by 0.09 and 0.16 electron than those in $BaFe_2S_3$, respectively. Therefore, the replacement of Ba^{2+} by K^{1+} does not really dope the iron sites by the nominal amount of 0.5 hole, but those holes mostly go to the S sites due to the partially covalent Fe-S bonds.

Since the electronic density of Fe is slightly lower in KFe_2S_3, the critical pressure should be higher according to the Bader charge analysis. To verify this expectation, the calculated crystal constants and magnetism (with pure GGA) are presented in Fig. 4 as a function of pressure. As shown in Fig. 4(a), the CX-AFM $(\pi,\pi,0)$ state is always the ground state if it is magnetically ordered. The suppression of the magnetic moment by pressure is shown in Fig. 4(b). The first-order character of the transition is similar to that observed in $BaFe_2S_3$. The critical pressure (~ 23 GPa) is indeed larger, as expected. The band gap of the CX-AFM phase reduces to zero at 17 GPa, inducing a semiconductor-to-metal transition. The metallic nonmagnetic phase above 23 GPa may be superconducting, according to previous experience with $BaFe_2S_3$. Of course, this reasoning is merely by analogy between similar materials

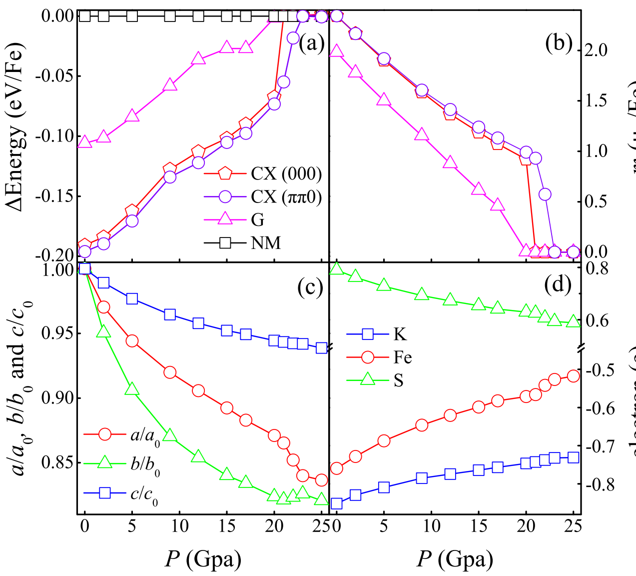

FIG. 4. DFT results of KFe_2S_3 as a function of pressure. (a) Energies (per Fe) of various magnetic orders. (b) Local magnetic moments of Fe. (c) Lattice constants normalized to the original ones for the CX state. (d) Bader charge analysis.

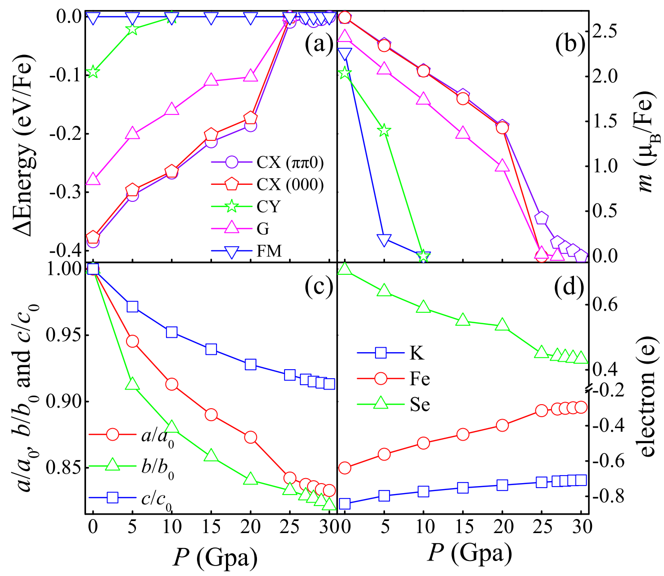

FIG. 5. DFT results of KFe_2Se_3 as a function of pressure. (a) Energies (per Fe) of various magnetic orders. (b) Local magnetic moments of Fe. (c) Lattice constants normalized to the original ones for the CX state. (d) Bader charge analysis.

because DFT cannot address superconductivity directly. The lattice constants under pressure, normalized to their ambient values, are shown in Fig. 4(c); they are also very similar to those reported for $BaFe_2S_3$. The Bader charge analysis applied to KFe_2S_3 under pressure leads to the same behavior as in $BaFe_2S_3$; namely, pressure enhances the local electronic density of the Fe sites, as shown in Fig. 4(d). There is also significant charge transfer (~ 0.24 electron per Fe) from S to Fe by increasing pressure from 0 to 25 GPa. Interestingly, the Bader charge densities at the critical pressures for magnetic quenching are almost identical (error bar $\delta < 0.005e$ in our calculations) for KFe_2S_3 and $BaFe_2S_3$, suggesting a similar physical mechanism for both compounds.

To summarize this section, our calculations here predict that KFe_2S_3 should be similar to $BaFe_2S_3$, regarding its magnetic ground state and its behavior under pressure. Thus, superconductivity is possible under higher pressure. By increasing pressure, the transfer of electrons from S to Fe occurs; namely, a self-doping process takes place that eventually could lead to superconductivity as in the canonical layered iron superconductors.

D. Pressure-induced transition in KFe_2Se_3

Since reducing the electronic density of the Fe atoms is a disadvantage to suppressing magnetism with increasing pressure, as demonstrated in KFe_2S_3 in which a higher pressure than for $BaFe_2S_3$ was needed to induce the metallic phase, it is natural to expect the opposite tendency in other AFe_2X_3 compounds that naturally have higher electronic density of the Fe atoms.

According to our Bader charge analysis, at ambient conditions the electronic density of the Fe atoms in KFe_2Se_3 (experimentally confirmed to display the CX-AFM order [23]) is higher than in the case of KFe_2S_3 by 0.12 electron and even higher than that in $BaFe_2S_3$ by 0.03 electron due to the weak electronegativity of Se. Then, a natural speculation arises: could it be that by increasing pressure KFe_2Se_3 is closer to metallicity, and thus perhaps also superconductivity, than $BaFe_2S_3$ is?

Despite the experimental studies by Caron *et al.* [23], DFT calculations for KFe_2Se_3 have not been performed to our knowledge. To remedy this problem, here, a pure GGA calculation has been carried out for KFe_2Se_3. At ambient conditions, the CX-AFM state is indeed the ground state [Fig. 5(a)]. The local moment of Fe is large, reaching the value of $2.65\mu_B$/Fe (slightly higher than the experimental one, $2.1\mu_B$/Fe [23]) at ambient conditions [Fig. 5(b)], which is a negative signal for metallicity and thus for potential superconductivity.

Under pressure, the quenching of the magnetic moment and semiconductor-metal transition indeed occurs. The gap of KFe_2Se_3 is about 0.56 eV at ambient conditions and is gradually closed by increasing pressure to 25 GPa. The required critical pressure for magnetic quenching reaches 29 GPa, even higher than that of KFe_2S_3. A different feature is that this magnetic phase transition seems to be more gradual, probably of second order or weak first order, rather than occurring by a sudden jump as observed in $BaFe_2S_3$ and KFe_2S_3. The Bader charge analysis is shown in Fig. 5(d) as a function of pressure. Furthermore, for the higher magnetic moment in KFe_2Se_3, the critical pressure should be higher to suppress the magnetism. Then, in this case additional charge transfer from Se to Fe may be required to suppress the magnetism.

To summarize this section, our DFT calculations have confirmed the CX-AFM magnetic ground state for KFe_2Se_3. Although KFe_2Se_3 has a relative high electronic density of the Fe atoms, its large gap and large moment make it even more difficult to induce a nonmagnetic metallic phase under pressure, and this magnetic-nonmagnetic transition may be of second order or weak first order. These different features may arise from the Se atoms, which are larger in size and weaker in their electronegativity.

IV. CONCLUSION

In this work, the magnetic and electronic properties of $BaFe_2S_3$, KFe_2S_3, and KFe_2Se_3 have been analyzed using first-principles calculations. The CX-AFM magnetic order is confirmed to be the common magnetic ground state for all these materials. The pressure-driven semiconductor-to-metal transition, as well as the antiferromagnetic-to-nonmagnetic transition, has been properly reproduced. Although the DFT technique cannot directly address a superconducting state, our study can provide helpful information to understand the superconducting transition of $BaFe_2S_3$ at high pressure (11 GPa), which is predicted to be a first-order transition. Our main conclusion is that the electron transfer from S to Fe, i.e., a self-doping process, may play a key role in tuning the magnetism in $BaFe_2S_3$ and eventually inducing metallicity and, potentially, superconductivity.

A similar first-order transition has also been predicted for KFe_2S_3, although the required critical pressure is higher (about 23 GPa). By contrast, although the magnetism can also be quenched in KFe_2Se_3, the required pressure (about 29 GPa) is even higher, and the transition seems to be of the second order or weak first order. Further experiments are encouraged to verify our predictions as well as the possible existence of metallicity, and perhaps superconductivity, in KFe_2S_3 and KFe_2Se_3.

ACKNOWLEDGMENTS

We acknowledge valuable discussions with R. Yu, H. Lu, and S. Chi. This work was primarily supported by the National Natural Science Foundation of China (Grant No. 11674055). E.D. was supported by the U.S. Department of Energy, Office of Basic Energy Sciences, Materials Sciences and Engineering Division. Most calculations were performed on Tianhe-2 at the National Supercomputer Center in Guangzhou (NSCC-GZ).

[1] Y. Kamihara, T. Watanabe, M. Hirano, and H. Hosono, J. Am. Chem. Soc. **130**, 3296 (2008).
[2] M. D. Lumsden and A. D. Christianson, J. Phys. Condens. Matter **22**, 203203 (2010).
[3] P. C. Dai, J. P. Hu, and E. Dagotto, Nat. Phys. **8**, 709 (2012).
[4] G. R. Stewart, Rev. Mod. Phys. **83**, 1589 (2011).
[5] D. C. Johnston, Adv. Phys. **59**, 803 (2010).
[6] E. Dagotto, Rev. Mod. Phys. **85**, 849 (2013).
[7] P. C. Dai, Rev. Mod. Phys. **87**, 855 (2015).
[8] Q. M. Si, R. Yu, and E. Abrahams, Nat. Rev. Mater. **1**, 16017 (2016).
[9] C. B. Bishop, A. Moreo, and E. Dagotto, Phys. Rev. Lett. **117**, 117201 (2016).
[10] S. Li, C. de la Cruz, Q. Huang, Y. Chen, J. W. Lynn, J. Hu, Y.-L. Huang, F.-C. Hsu, K.-W. Yeh, M.-K. Wu, and P. C. Dai, Phys. Rev. B **79**, 054503 (2009).
[11] C.-Y. Moon and H. J. Choi, Phys. Rev. Lett. **104**, 057003 (2010).
[12] F. Ma, W. Ji, J. Hu, Z.-Y. Lu, and T. Xiang, Phys. Rev. Lett. **102**, 177003 (2009).
[13] R. Yu and Q. M. Si, Phys. Rev. Lett. **115**, 116401 (2015).
[14] W. Li, H. Ding, P. Deng, K. Chang, C. L. Song, K. He, L. L. Wang, X. C. Ma, J. P. Hu, X. Chen, and Q. K. Xue, Nat. Phys. **8**, 126 (2012).
[15] W. Li, S. Dong, C. Fang, and J. P. Hu, Phys. Rev. B **85**, 100407 (2012).
[16] Y. Zhang, H. M. Zhang, Y. K. Weng, L. F. Lin, X. Y. Yao, and S. Dong, Phys. Status Solidi RRL **10**, 757 (2016).
[17] W. Bao, Q. Z. Huang, G. F. Chen, M. A. Green, D. M. Wang, J. B. He, and Y. M. Qiu, Chin. Phys. Lett. **28**, 086104 (2011).
[18] F. Ye, S. Chi, W. Bao, X. F. Wang, J. J. Ying, X. H. Chen, H. D. Wang, C. H. Dong, and M. H. Fang, Phys. Rev. Lett. **107**, 137003 (2011).
[19] W.-G. Yin, C.-C. Lee, and W. Ku, Phys. Rev. Lett. **105**, 107004 (2010).
[20] A. Krzton-Maziopa, E. Pomjakushina, V. Pomjakushin, D. Sheptyakov, D. Chernyshov, V. Svitlyk, and K. Conder, J. Phys. Condens. Matter **23**, 402201 (2011).
[21] B. Saparov, S. Calder, B. Sipos, H. Cao, S. Chi, D. J. Singh, A. D. Christianson, M. D. Lumsden, and A. S. Sefat, Phys. Rev. B **84**, 245132 (2011).
[22] J. M. Caron, J. R. Neilson, D. C. Miller, A. Llobet, and T. M. McQueen, Phys. Rev. B **84**, 180409(R) (2011).
[23] J. M. Caron, J. R. Neilson, D. C. Miller, K. Arpino, A. Llobet, and T. M. McQueen, Phys. Rev. B **85**, 180405(R) (2012).
[24] H. Lei, H. Ryu, A. I. Frenkel, and C. Petrovic, Phys. Rev. B **84**, 214511 (2011).
[25] R. Arita, H. Ikeda, S. Sakai, and M.-T. Suzuki, Phys. Rev. B **92**, 054515 (2015).
[26] M. Wang, M. Yi, S. J. Jin, H. C. Jiang, Y. Song, H. Q. Luo, A. D. Christianson, C. de la Cruz, E. Bourret-Courchesne, D. X. Yao, D. H. Lee, and R. J. Birgeneau, Phys. Rev. B **94**, 041111(R) (2016).
[27] N. D. Patel, A. Nocera, G. Alvarez, R. Arita, A. Moreo, and E. Dagotto, Phys. Rev. B **94**, 075119 (2016).
[28] E. Dagotto, Rev. Mod. Phys. **66**, 763 (1994).
[29] E. Dagotto, Rep. Prog. Phys. **62**, 1525 (1999).
[30] S. Dong, J.-M. Liu, and E. Dagotto, Phys. Rev. Lett. **113**, 187204 (2014).
[31] S. Dong, J.-M. Liu, S. W. Cheong, and Z. F. Ren, Adv. Phys. **64**, 519 (2015).
[32] S. W. Lovesey, D. D. Khalyavin, and G. van der Laan, Phys. Scr. **91**, 015803 (2016).
[33] H. Takahashi, A. Sugimoto, Y. Nambu, T. Yamauchi, Y. Hirata, T. Kawakami, M. Avdeev, K. Matsubayashi, F. Du, C. Kawashima, H. Soeda, S. Nakano, Y. Uwatoko, Y. Ueda, T. J. Sato, and K. Ohgushi, Nat. Mater. **14**, 1008 (2015).

[34] Z. S. Gönen, P. Fournier, V. Smolyaninova, R. Greene, F. M. Araujo-Moreira, and B. Eichhorn, Chem. Mater. **12**, 3331 (2000).
[35] W. M. Reiff, I. E. Grey, A. Fan, Z. Eliezer, and H. Steinfink, J. Solid State Chem. **13**, 32 (1975).
[36] T. Yamauchi, Y. Hirata, Y. Ueda, and K. Ohgushi, Phys. Rev. Lett. **115**, 246402 (2015).
[37] M. T. Suzuki, R. Arita, and H. Ikeda, Phys. Rev. B **92**, 085116 (2015).
[38] G. Kresse and J. Hafner, Phys. Rev. B **47**, 558 (1993).
[39] G. Kresse and J. Furthmüller, Phys. Rev. B **54**, 11169 (1996).
[40] P. E. Blöchl, O. Jepsen, and O. K. Andersen, Phys. Rev. B **49**, 16223 (1994).
[41] J. P. Perdew, K. Burke, and M. Ernzerhof, Phys. Rev. Lett. **77**, 3865 (1996).
[42] A. A. Mostofi, J. R. Yates, Y. S. Lee, I. Souza, D. Vanderbilt, and N. Marzari, Comput. Phys. Commun. **178**, 685 (2007).
[43] P. Hansmann, R. Arita, A. Toschi, S. Sakai, G. Sangiovanni, and K. Held, Phys. Rev. Lett. **104**, 197002 (2010).
[44] I. I. Mazin, M. D. Johannes, L. Boeri, K. Koepernik, and D. J. Singh, Phys. Rev. B **78**, 085104 (2008).
[45] I. I. Mazin and M. D. Johannes, Nat. Phys. **5**, 141 (2009).
[46] S. Dong, R. Yu, J.-M. Liu, and E. Dagotto, Phys. Rev. Lett. **103**, 107204 (2009).
[47] J. Ferber, Y. Z. Zhang, H. O. Jeschke, and R. Valentí, Phys. Rev. B **82**, 165102 (2010).
[48] M. Yi, D. H. Lu, J. G. Analytis, J. H. Chu, S. K. Mo, R. H. He, M. Hashimoto, R. G. Moore, I. I. Mazin, D. J. Singh, Z. Hussain, I. R. Fisher, and Z.-X. Shen, Phys. Rev. B **80**, 174510 (2009).
[49] L. Ortenzi, H. Gretarsson, S. Kasahara, Y. Matsuda, T. Shibauchi, K. D. Finkelstein, W. Wu, S. R. Julian, Y.-J. Kim, I. I. Mazin, and L. Boeri, Phys. Rev. Lett. **114**, 047001 (2015).
[50] Y. T. Tam, D. X. Yao, and W. Ku, Phys. Rev. Lett. **115**, 117001 (2015).
[51] R. F. W. Bader, *Encyclopedia of Computational Chemistry* (Wiley, Chichester, UK, 2002).
[52] W. Tang, E. Sanville, and G. Henkelman, J. Phys. Condens. Matter **21**, 084204 (2009).
[53] G. Henkelman, A. Arnaldsson, and H. Jónsson, Comput. Mater. Sci. **36**, 354 (2006).
[54] E. Dagotto and T. M. Rice, Science **271**, 618 (1996).
[55] R. H. Mitchell, K. C. Ross, and E. G. Potter, J. Solid State Chem. **177**, 1867 (2004).